Matter

CellPress
OPEN ACCESS

Article

Integration of kinks and creases enables tunable folding in meta-ribbons

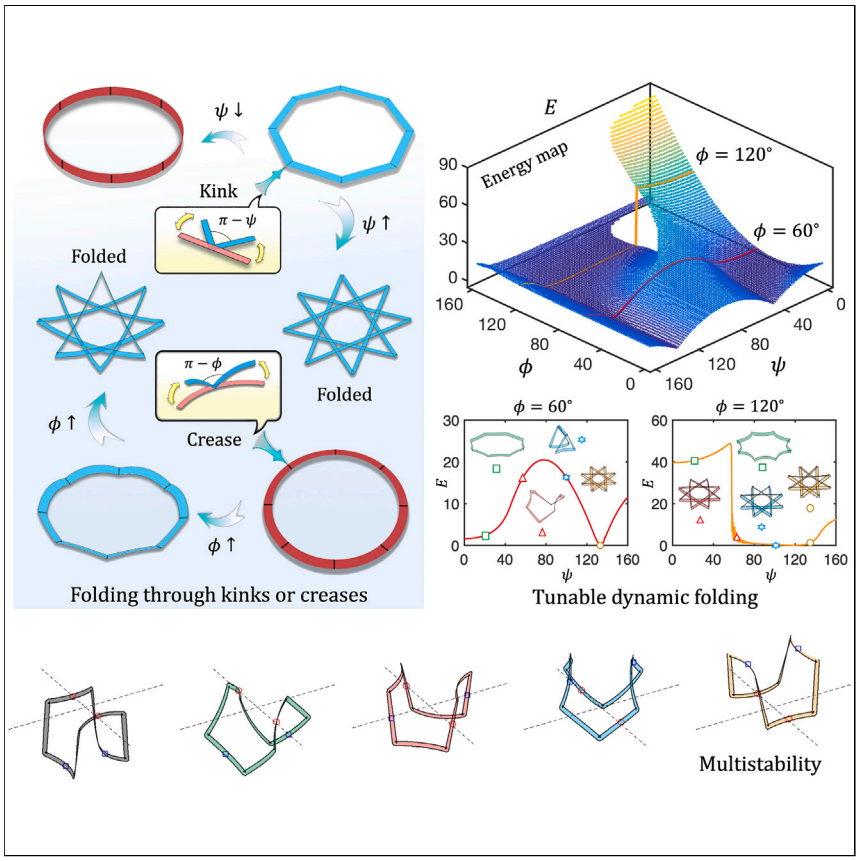

We introduce the concept of the "meta-ribbon" by integrating both in-plane kinks and out-of-plane creases in slender structures. Our analysis reveals that kinks or creases can trigger either continuous or snapping folding, stemming from different types of bifurcations. By integrating them into the meta-ribbon and carefully engineering their arrangement, we can achieve tunable folding between continuous and snapping modes.

Weicheng Huang, Tian Yu, K. Jimmy Hsia, Sigrid Adriaenssens, Mingchao Liu

jhyutian@vt.edu (T.Y.)
m.liu.2@bham.ac.uk (M.L.)

Highlights

The nonlinear folding behaviors of annular ribbons are comprehensively investigated

The folding mechanism and bifurcation type of elastic annular ribbons are uncovered

The meta-ribbon is created by integrating in-plane kinks and out-of-plane creases

The tunable dynamic folding behavior of a meta-ribbon is achieved

Benchmark
First qualification/assessment of material properties and/or performance

Huang et al., Matter 7, 3007–3023
September 4, 2024
Published by Elsevier Inc.
https://doi.org/10.1016/j.matt.2024.04.031

Matter

CellPress
OPEN ACCESS

Article

Integration of kinks and creases enables tunable folding in meta-ribbons

Weicheng Huang,[1] Tian Yu,[2,*] K. Jimmy Hsia,[3,4] Sigrid Adriaenssens,[5] and Mingchao Liu[3,6,7,*]

SUMMARY

Foldable structures find diverse applications. Folding of thin structures into compact shapes involves the interplay of nonlinear mechanics and topology. In this study, we employ discrete models, theoretical analysis, and tabletop experiments to systematically investigate the geometrically nonlinear folding process of ring-shape elastic ribbons through in-plane kinks and out-of-plane creases. We find that kinks initiate continuous folding through supercritical bifurcation, while creases trigger abrupt snapping via subcritical bifurcation. Master curves that summarize energy landscapes for ribbons with varying numbers of kinks and creases are obtained. By integrating kinks and creases, a "meta-ribbon" can be created, which shows the tunable folding behavior, transitioning from continuous to snapping, or vice versa, by strategically engineering the in-plane and out-of-plane angles guided by the constructed energy map. As a product of folding, we demonstrate the snapping-induced vibration accomplished with dynamic folding, as well as the multistability of meta-ribbons with saddle-like configurations and their transformation.

INTRODUCTION

Folding of slender structures is an intriguing and transformative phenomenon occurring at different scales and holding immense scientific and engineering potential.[1–3] From natural substances found in the biological realm[4,5] to artificial structures inspired by origami principles,[6–8] the folding of slender structures offers a rich and fertile ground for exploration. This phenomenon encompasses a diverse range of materials, including biological tissues, polymers, metals, and composites, giving rise to folded configurations with unique characteristics such as compact shapes, small volumes, and exceptional mechanical and physical performances.[9,10] The intricate folding patterns and behaviors exhibited by slender structures have far-reaching implications in both understanding natural phenomena and inspiring the design of engineering structures. By exploring and harnessing the principles of folding, experts in the field can unlock new frontiers in design, manufacturing, and functional materials development, potentially revolutionizing fields as diverse as healthcare, aerospace, robotics, and sustainable architecture.[11–15]

In nature, slender structures undergo crucial folding processes that are essential for their functionality, and some examples include DNA/RNA, proteins, and the brain folding into three-dimensional (3D) conformations, which play critical roles in dictating their biological functions,[16–20] as well as the folding of leaves and wings in response to environmental stimuli, which allows plants and insects to adapt and thrive.[21–24] Studying these folding mechanisms, from molecular to

PROGRESS AND POTENTIAL

Exploring how thin structures fold can lead to innovative technologies in fields like soft robotics, flexible electronics, and space deployable systems. By studying the mechanics of folding in elastic ribbons, through discrete model, theory, and experiment, we uncovered that different types of folds, i.e., in-plane kinks and out-of-plane creases, initiate folding in distinct ways and correspond to different types of bifurcation. We also found that by combining these folds strategically, we can create "meta-ribbons," which can fold smoothly or abruptly based on how they are engineered. This tunability opens doors for advantages like controllable dynamic folding and transitions among different stable states, offering exciting possibilities for future technologies.

macroscopic scales, offers valuable insights into the fundamental principles governing biological systems. Inspired by nature's ingenious folding strategies, origami/kirigami principles, which enable the transformation of two-dimensional (2D) sheets into intricate 3D shapes, have been adopted to engineer foldable structures with remarkable properties.[25–28] Ring origami, a notable approach among these foldable structures, involves folding ring-shape rods or ribbons into deployable/reconfigurable functional structures.[29–34] These origami-inspired foldable structures exhibit exceptional foldability, scalability, and versatility, making them well suited for applications across various scales.

Understanding the mechanical properties of foldable structures is crucial for achieving precise control and functionality. The folding process significantly impacts the stiffness, flexibility, and compatibility of folded structures, paving the way for the creation of resilient yet lightweight designs. Mastering the mechanics of folding and managing the folding pathways is vital for practical applications of foldable structures.[35–37] For certain foldable structures like reconfigurable origami and kirigami, rapid folding, especially through snapping folding, is desirable.[38–40] However, the snap-through process can introduce significant vibrations, especially in underdamped situations,[41] which can be detrimental in precision instruments and space engineering. Additionally, achieving specific intermediate configurations along the unstable branch of the bifurcation diagram can be challenging, limiting certain applications.[42] Conversely, continuous folding without snapping, which is usually more suitable for certain applications like space engineering,[43,44] is achievable through careful origami pattern design.[45] However, achieving tunable folding behaviors transitioning from snapping to continuous folding, or vice versa, within a single structure remains a challenge to date.

In this study, we present a comprehensive investigation on the folding behavior of slender elastic structures, in particular ring-shape ribbons. As common geometric manipulation strategies, in-plane kinks (associated with a sudden change in the in-plane bending angle and akin to the hinged joint found in linkage structures) and out-of-plane creases (corresponding to a discontinuity in out-of-plane angle and resembling a hinge—a crucial component in origami structures) are introduced to achieve a tunable folding process in flexible structures. To investigate the nonlinear folding behaviors, an efficient and robust discrete model is developed based on the well-established discrete elastic rod (DER) algorithm with C^0 continuity.[46,47] A theoretical model based on Kirchhoff's rod theory together with the Dirac delta function[48] is adopted for cross-validation. Our analysis reveals that the folding process of a polygonal ribbon through multiple in-plane kinks is continuous, and it corresponds to supercritical bifurcation, while the folding of an annular ribbon through multiple out-of-plane creases is not continuous, accompanied by snapping and governed by subcritical bifurcation. By integrating both kinks and creases, the folding process of a ring-shape ribbon can be tuned to achieve either snapping folding or continuous folding by choosing an appropriate strategy guided by the energy map of the system. Therefore, this type of foldable structure is referred to as "meta-ribbon." Our dynamic analysis demonstrates that the vibration generated in the folding process can be eliminated by tuning the snapping folding to continuous folding. Moreover, the transformations between multiple stable/unstable configurations of meta-ribbons are also explored. Our primary objective is to uncover the fundamental principles and mechanics governing foldable structures. By doing so, we aim to establish a solid groundwork for future advancements in structural design and manufacturing techniques and the development of foldable structures with pluripotent functionalities.

[1]School of Engineering, Newcastle University, NE1 7RU Newcastle upon Tyne, UK

[2]Department of Mechanics and Aerospace Engineering, Southern University of Science and Technology, Shenzhen 518055, China

[3]School of Mechanical and Aerospace Engineering, Nanyang Technological University, Singapore 639798, Republic of Singapore

[4]School of Chemistry, Chemical Engineering and Biotechnology, Nanyang Technological University, Singapore 639798, Republic of Singapore

[5]Department of Civil and Environmental Engineering, Princeton University, Princeton, NJ 08544, USA

[6]Department of Mechanical Engineering, University of Birmingham, B15 2TT Birmingham, UK

[7]Lead contact

*Correspondence: jhyutian@vt.edu (T.Y.), m.liu.2@bham.ac.uk (M.L.)

https://doi.org/10.1016/j.matt.2024.04.031

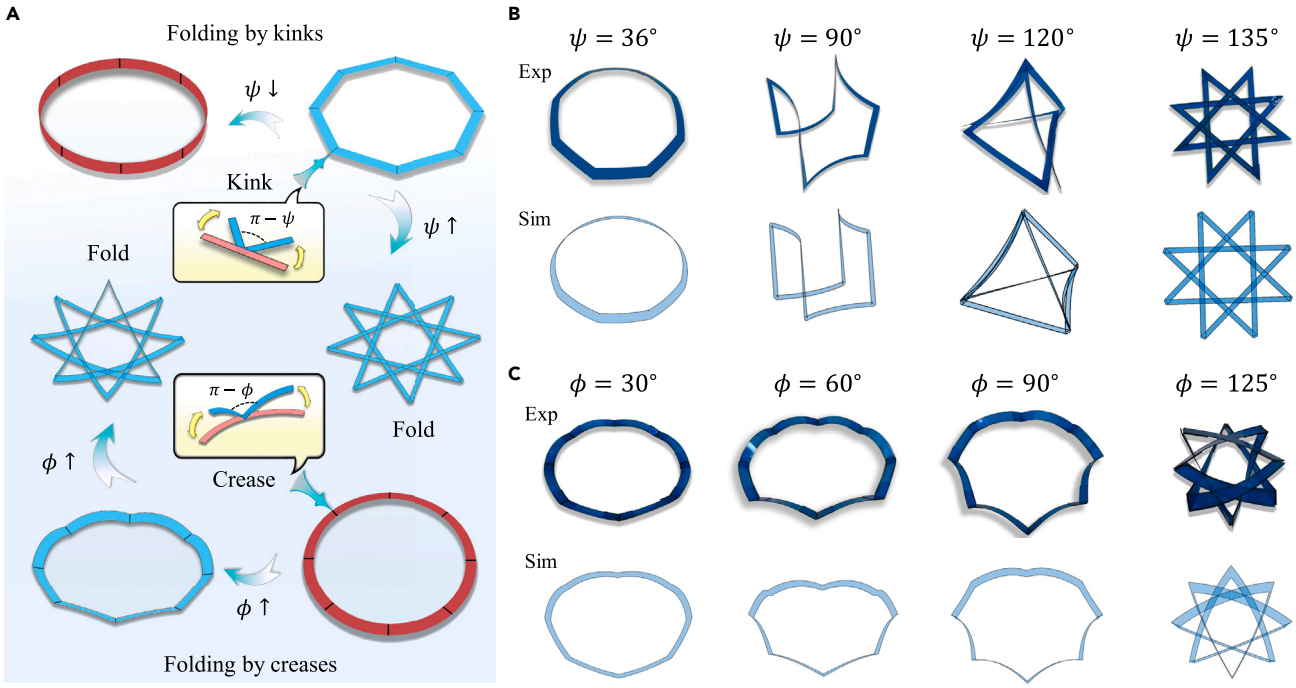

Figure 1. Introduction of kinks and creases for the folding of (ring-shape) meta-ribbons

(A) Schematic diagram of the folding of a polygonal ribbon by kinks (with the angle of kink, ψ) and a circular ribbon by creases (with the angle of crease, ϕ).

(B) Folding a polygonal ribbon through in-plane kinks (with number of kinks, $N^c = 8$).

(C) Folding an annular ribbon through out-of-plane creases (with number of creases, $N_c = 8$).

RESULTS

Here, we present a geometric design strategy aimed at manipulating the nonlinear mechanics involved in the folding process of ring-shape elastic ribbons. This is achieved by introducing in-plane kinks and out-of-plane creases, resulting in the formation of polygonal frames and creased annuli, respectively. Ultimately, both the frames and annuli fold to form polygons with acute angles, as illustrated in Figure 1A. By leveraging the distinct characteristics of kinks and creases, our design strategy allows us to investigate the folding mechanism of ribbons, with the turning angles playing a crucial role in this process. A ring-shape ribbon can undergo folding via two distinct mechanisms: in-plane kinks (Figure 1B) or out-of-plane creases (Figure 1C). The introduction of kinks and creases to thin ribbons disrupts the rotational symmetry of the ring shape, resulting in a finite number of stable saddle-shaped configurations rather than a continuous range of states with identical shape and energy. By combining kinks and creases, we can tailor the folding process to exhibit either a continuous or snapping behavior. We substantiate our findings with experimental observations and simulation results obtained from both discrete and continuous models, showcasing the generic nature of the folding behavior in discontinuous annuli. The design of kink and crease angles allows for precise tuning of this behavior. Detailed information regarding the discrete simulations and the tabletop experiments can be found in the experimental procedures; the continuous model is briefly described in the experimental procedures and detailed in supplemental experimental procedures section 1. Furthermore, we provide a comprehensive cross-validation by systematically comparing the results obtained from both models in supplemental experimental procedures section 2 (see Figure S1).

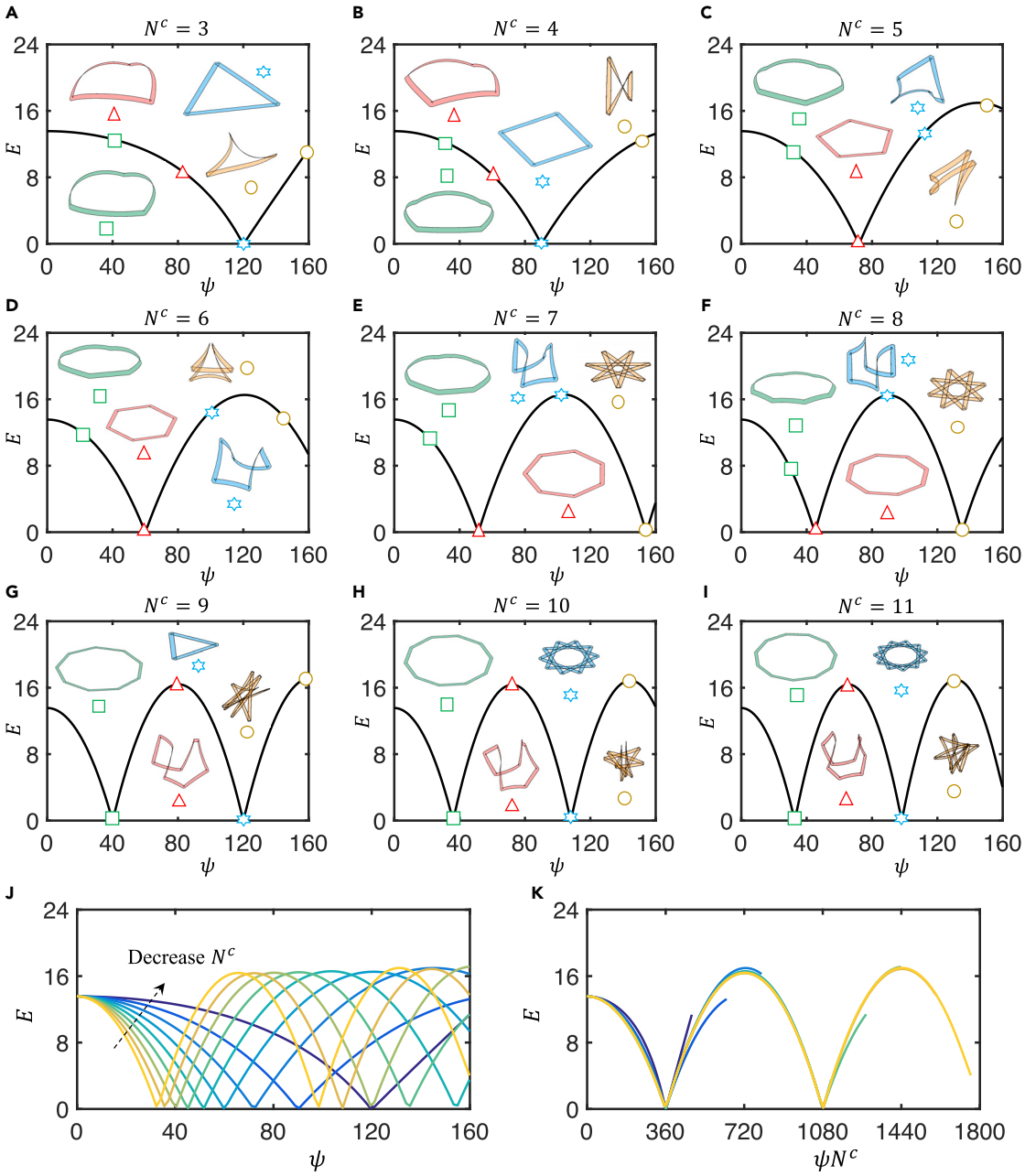

Figure 2. Folding of elastic polygonal ribbon via in-plane kinks

(A–I) The total elastic energy, E, as a function of the in-plane angle, ψ, for different number of kinks, N^c: N^c = (A) 3, (B) 4, (C) 5, (D) 6, (E) 7, (F) 8, (G) 9, (H) 10, and (I) 11.

(J) Combined data for (A)–(I).

(K) The total energy, E, vs. the total folding angle, ψN^c.

Folding through in-plane kinks

The folding mechanism of ring-shape elastic ribbons through in-plane kinks is similar to the overcurvature of an annular strip (see supplemental experimental procedures section 3; Figure S2),[29,48] with the uniformly distributed geodesic curvature in circles localized at the vertices of polygonal frames (Figure 2). Figures 2A–2I present the elastic energy (E) as a function of kink angle (ψ) for the elastic polygonal ribbons

with different numbers of kinks (N^c), i.e., N^c varies from 3 to 11. The energy, E, which is normalized by the torsional rigidity, GJ, is given by the discrete Kirchhoff model as

$$E = \sum_{i=0}^{N-1} \frac{1}{2} l\left[a_i(\kappa_{1,i} - \bar{\kappa}_{1,i})^2 + b_i(\kappa_{2,i} - \bar{\kappa}_{2,i})^2 + c_i(\kappa_{3,i} - \bar{\kappa}_{3,i})^2\right]\Delta l_i, \quad \text{(Equation 1)}$$

where l is the ribbon length, $\kappa_{1,i}$ is the discrete in-plane curvature of the i-th node, $\kappa_{2,i}$ is the discrete out-of-plane curvature, $\kappa_{3,i}$ is the twisting curvature, Δl_i is its Voronoi length, and a_i, b_i, and c_i are the normalized local stiffnesses (i.e., $\{a_i, b_i, c_i\} = \{EI_{1,i}, EI_{2,i}, GJ_i\}/GJ$, where $EI_{1,i}$, $EI_{2,i}$, and GJ_i are the two local bending rigidities and the torsional rigidity, respectively). It is also worth noting that the kink angle ψ can be specified by using the discrete in-plane curvature, i.e., if a ψ is required at the i-th node, then we will transfer the ψ into the discrete in-plane curvature,

$$\bar{\kappa}_{1,i} = 2\frac{\tan(\psi_i/2)}{\Delta l_i}, \quad \text{(Equation 2)}$$

and then use a relatively large stiffness a_i to achieve $\kappa_{1,i} = \bar{\kappa}_{1,i}$. When $\psi = 2\pi/N^c$, elastic polygons remain in plane and have vanishing energy, representing the ground state, as in the case of $\psi = 120^\circ$ for $N^c = 3$ (see Figure 2A). With decreasing or increasing ψ, the structure buckles into a dome-like or saddle-like shape, respectively.[49] On the one hand, when $\psi < 2\pi/N^c$, the structure buckles into a self-stressed dome-like shape, and specifically, $\psi = 0$ makes a circular cylinder. On the other hand, with $\psi > 2\pi/N^c$, the structure buckles into a saddle-like shape, and more interestingly, it further folds into a multilayered polygonal structure with an odd number of revolutions, N_{rev} (i.e., $N_{rev} = 3,5,7$, etc.), with each revolution representing a full rotation of 2π. If N^c is divisible by N_{rev}, then we obtain a N^c/N_{rev}-side polygon with N_{rev} revolutions, which are fully overlapped. For example, a three-revolution ($N_{rev} = 3$) triangular shape ($N^c/N_{rev} = 3$) can be achieved when folding a polygonal ribbon by ($N^c = $) 9 kinks with $\psi = 6\pi/9 = 120^\circ$ (see Figure 2G). However, if N^c is not divisible by N_{rev}, then the folded geometry would be a N^c-side polygon with partial overlap. A representative dynamic rendering for the kink-induced folding of a polygonal ribbon with $N^c = 8$ is available in Video S1. It is worth noting that the folding mechanism of an elastic polygonal ribbon with $N_{rev}|N^c (N_{rev} \geq 3)$ is similar to the higher-order folded state in ring origami.[32,49] For example, the higher-order folded state with $N^c/N_{rev} = 3$ is similar to the triply covered folding of circular strips,[29] i.e., the folded configuration is with $N^c/3$ sides.

In the current study, the folding angle ψ is limited to vary in the range $[0^\circ, 160^\circ]$. It is clearly seen that, for $\psi = 2\pi/N^c$ and $\psi = 6\pi/N^c$, the structures correspond to the flat polygon (with one revolution) and the folded multilayered polygonal structure (with three revolutions), respectively, and both are energy free. From Figures 2A–2I, we can see that the elastic energy of the system E evolves nonmonotonically with the increase of the kink angle ψ. In Figure 2J, we combine all cases (with $N^c = 3$–11) together, and it shows a similar trend for all these cases. By re-scaling the x axis as ψN^c, which measures the total folding angle, we observe the collapse of all the curves on a single master curve, as depicted in Figure 2K. This collapse indicates that the energy states of the kink-induced folding process of polygonal ribbons are generic regardless of the N^c introduced. For the energy-free flat one-revolution and three-revolution configurations, the total folding angles are $2\pi(360^\circ)$ and $6\pi(1080^\circ)$ for all cases, respectively. According to the stability analysis, as shown in Figure S3, the out-of-plane buckling behavior during the folding process is governed by a supercritical pitchfork bifurcation (see supplemental experimental procedures section 4 and Figure S3 for a more detailed discussion). This is the essential cause of the continuous folding.

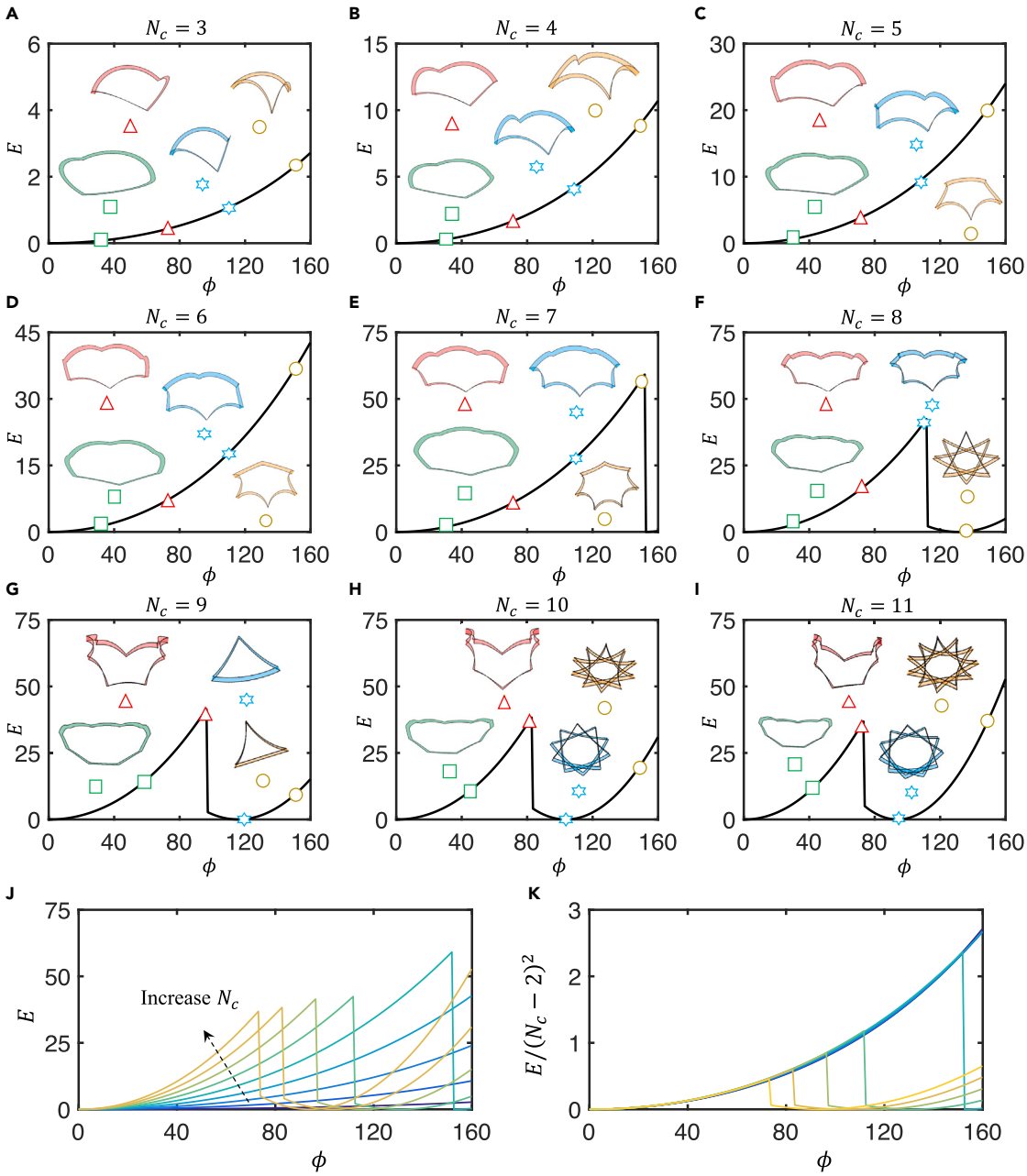

Figure 3. Folding of elastic annular ribbon via out-of-plane creases

(A–I) The total elastic energy, E, as a function of the out-of-plane angle, ϕ, for different number of creases, N_c: N_c = (A) 3, (B) 4, (C) 5, (D) 6, (E) 7, (F) 8, (G) 9, (H) 10, and (I) 11.

(J) Combined data for (A)–(I).

(K) The normalized total energy, $E/(N_c - 2)^2$, as a function of the folding angle, ϕ.

Folding through out-of-plane creases

As demonstrated in Figure 1, the folding of ring-shape ribbons can also be achieved by introducing out-of-plane creases. In particular, annular ribbons can be folded into different patterns through the introduction of radial creases.[48] Figures 3A–3I present numerical simulation results of the normalized total elastic energy, E, of the folded annular ribbons with different numbers of creases, N_c, from 3 to 11, and crease

angles, ϕ. Similar to the ψ in previous cases, the ϕ can be also specified by using the discrete out-of-plane curvature, i.e., if a ϕ is required at the i-th node, then we will transfer the ϕ into the discrete out-of-plane curvature,

$$\bar{\kappa}_{2,i} = 2\frac{\tan(\phi_i/2)}{\Delta l_i}, \qquad \text{(Equation 3)}$$

and then use a relatively large stiffness b_i to achieve $\kappa_{2,i} = \bar{\kappa}_{2,i}$. A vanishing $\phi = 0^\circ$ corresponds to a flat stress-free annulus, and the ϕ is also limited to vary in the range $[0^\circ, 160^\circ]$. Note that all the annular ribbons are rotationally symmetric initially. However, with the increase of the ϕ, they may evolve into curved shapes with the symmetry broken. With $N_c \leq 6$, we can observe a continuous deformation path with the increase of the ϕ. However, for $N_c \geq 7$, creased annuli fold, via a sudden jump, into a compacted shape at a certain ϕ. Similar to the kink-induced folding, we can also notice that the folded geometry depends on the N_c. For the case with N_{rev}/N_c ($N_{rev} = 3, 5, 7$, etc.), a fully overlapped N_c/N_{rev}-side polygon with N_{rev} revolutions can be obtained. For example, as shown in Figure 3G, a triangular shape ($N_c/N_{rev} = 3$) with three revolutions ($N_{rev} = 3$) can be obtained by folding an annular ribbon through ($N_c = $) 9 creases with angle $\phi = 6\pi/9 = 120^\circ$. Otherwise, the folded geometry would be an N_c-side polygon with partial overlap, while N_c is not divisible by N_{rev}. A representative dynamic rendering for the crease-induced folding of an annular ribbon with $N_c = 8$ is available in Video S2.

Again, from Figures 3A–3I, we can find that the relationship between the total energy E and the crease angle ϕ for all cases with a different crease number N_c share a similar trend. In Figure 3J, we combine all cases together, and a similar trend can be further confirmed. It is clearly seen that, with the same ϕ, the ribbon with more creases shows larger E. This can be understood as the total energy being the sum of the energy generated by each crease, and more creases result in more energy. Quantitatively, $N_c = 2$ corresponds to the zero-energy mode, i.e., there is no elastic energy existing in the annular strip with two symmetric radial creases, as we ignore the energy at the creases, while $N_c \geq 3$ corresponds to the deformable modes. Interestingly, by normalizing the energy E with $(N_c - 2)^2$, as shown in Figure 3K, the energy vs. folding angle curves for all cases before snapping collapse onto a single master curve. Also, similar to kink-induced folding, the second energy-free configuration after folding occurs when the creased angle equals $6\pi/N_c$, e.g., the total deformable energy is zero when $\phi = 120^\circ$ for the strip with ($N_c = $) 9 creases. Upon further investigation into the snapping by conducting numerical continuation, we find that it is caused by a subcritical pitchfork bifurcation (see Figure S4 in supplemental experimental procedures section 5), and the resultant folding process involves a sudden configuration change, contrasting with the previous continuous folding operation induced by kinks.

Folding through both kinks and creases

So far, we understand that the continuous folding of the polygonal elastic ribbons with kinks is governed by a supercritical bifurcation, while the folding of annular ribbons with creases is caused by a subcritical bifurcation that results in a sudden state change. We further investigate the folding behavior of the ring-shape ribbon through combined in-plane kinks and out-of-plane creases. Here, a polygonal ribbon with 8 folds is considered for demonstration, where both kink and crease are introduced at each fold position, i.e., $N^c = N_c = 8$. By performing systematic numerical simulation, a comprehensive energy map for the folding of the ribbon by changing both the kink angle ψ and crease angle ϕ is obtained, as shown in Figure 4A. Here, both the ψ and ϕ are specified by using the discrete bending

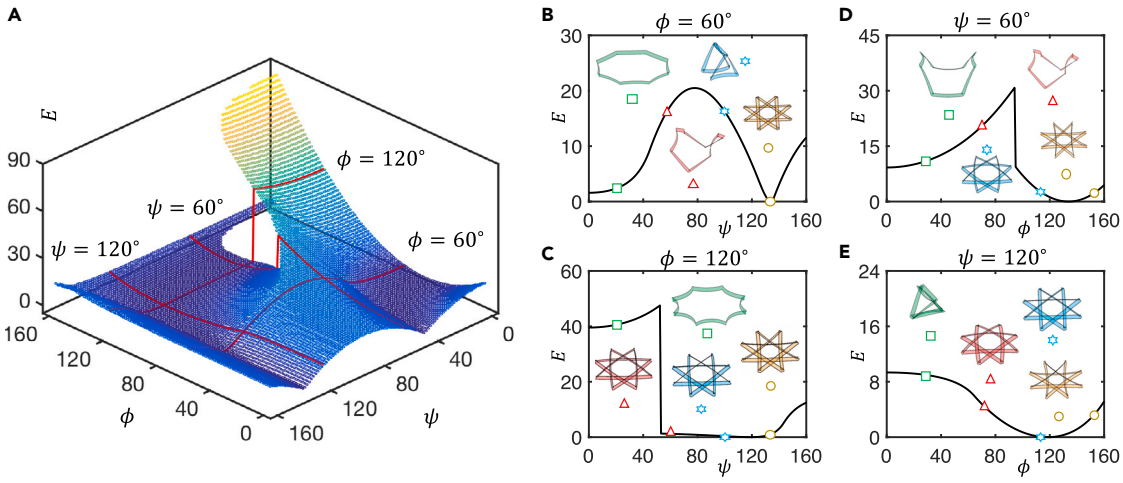

Figure 4. Folding of a regular octagon by the integration of both kinks and creases

(A) Dependence of the total elastic energy, E, on both the in-plane angle, ψ, and the out-of-plane angle, ϕ, with a fixed number of kinks and creases, $N_c = N^c = 8$.

(B and C) The E as a function of the ψ with a specified ϕ: ϕ = (B) 60° and (C) 120°.

(D and E) The E as a function of the ϕ with a specified ψ: ψ = (D) 60° and (E) 120°.

curvatures in a manner similar to the previous approach. Particularly, we can note that $\{\psi = 45^\circ, \phi = 0\}$ and $\{\psi = 135^\circ, \phi = 0\}$ correspond to the regular octagon and the fully folded 8-side polygon, respectively, which are two ground states, and their elastic energies E are both zero.

While most areas of the energy map are continuous, Figure 4A shows that there is a discontinuous region of the energy distribution within the $E(\psi, \phi)$ plane, which indicates that the folding process could be discontinuous, i.e., with snapping, once the folding path passes through this region. In particular, we take several examples for demonstration. When the crease angle ϕ is fixed as a smaller number, e.g., $\phi = 60^\circ$, the kink-induced folding is continuous (refer to Figure 4B). However, if the ϕ is selected as a larger number (such as $\phi = 120^\circ$), the energy would show a sudden decrease as a function of the kink angle ψ (see Figure 4C). On the other hand, we show the dependence of total energy E on the crease angle ϕ with a fixed kink angle ψ. When the ψ is small, the folding caused by the crease is again abrupt (refer to Figure 4D for $\psi = 60^\circ$); nevertheless, when the ψ is set to be a larger number (e.g., $\psi = 120^\circ$), the overall folding process due to the change of ϕ would be continuous (see Figure 4E for details). In all, the folding process of the ring-shape ribbon is tunable, and the desired folding process can be achieved if a suitable path is selected based on the energy map computed by our discrete model. We therefore refer to this type of foldable ribbon as a meta-ribbon. Notably, while our primary focus is on understanding the fundamental folding mechanisms through theory and numerical modeling, the physical implementation of both kinks and creases is feasible, either via mechanical mechanisms or by adopting smart materials such as liquid crystal elastomers.

Dynamic folding behaviors of a meta-ribbon

According to our prior knowledge, it is known that the sharp state transition in multi- or bistable structures during snapping can normally generate vibrations, particularly in underdamped situations,[41] due to the sudden release of elastic energy. This snapping-induced vibration is undesirable for particular applications, such as the

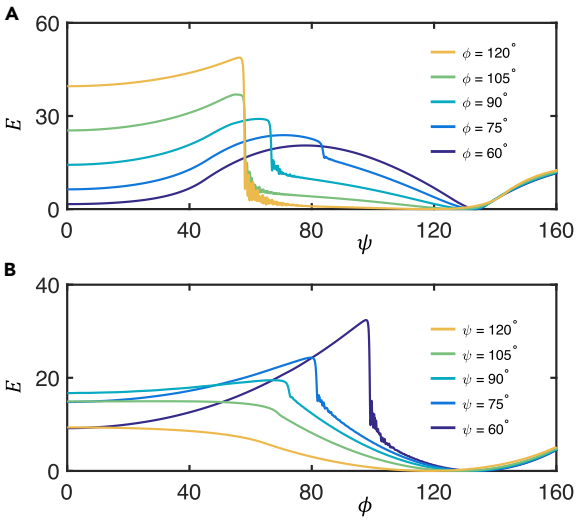

Figure 5. Dynamic folding behaviors of a meta-ribbon through both kinks and creases (N_c = N^c = 8)

(A) Folding through in-plane kinks with a fixed crease angle, ϕ.

(B) Folding through out-of-plane creases with a fixed kink angle, ψ.

deployment of foldable structures in precision instruments and space engineering. However, continuous folding is more smooth and stable for given damping but is also by no means "perfect," which normally corresponds to the slow process.[41] The results in Figure 4 indicate that we can manipulate the folding process through different paths to achieve either snapping or continuous folding. Therefore, we can expect to suppress the vibration by choosing the folding path without snapping but also have to sacrifice some of the folding speed.

To prove this concept, we investigate the dynamic folding process of meta-ribbons through both kinks and creases (see supplemental experimental procedures section 6 for more details about the dynamic analysis). In Figure 5A, we present the energy evolution for different folding paths with varying kink angle ψ and fixed crease angle ϕ. For a smaller ϕ, e.g., $\phi = 60^\circ$, the dynamic folding process is smooth (as shown in Video S3). As the ϕ increases, the transition becomes sharper; when there is a sudden change, e.g., $\phi = 120^\circ$ (see Video S4), the system would experience snapping folding accompanied by significant vibrations. Generally, the sharper jump corresponds to larger vibrations, and the magnitude and duration of the vibration would increase if the energy gap is relatively large. For the folding process with varying crease angle ϕ and fixed kink angle ψ, a similar trend can be observed in Figure 5B, i.e., a smooth curve can be found if the folding path is continuous, e.g., $\psi = 60^\circ$ (see Video S5), while vibrations would emerge if the structure sharply jumps from one equilibrium configuration to another, such as the case with $\psi = 120^\circ$ (as shown in Video S6). Note that the vibration can eventually dissipate as the damping force is included in the dynamic system. The effect of the folding speed has also been explored, and the results are summarized in Figure S5 in supplemental experimental procedures section 6. It has been found that a significant delay appears in the situation of snapping folding under different folding speeds, while continuous folding is loading-rate insensitive. The findings here may provide new insight into the optimal design of a foldable meta-ribbon, for instance, choosing a suitable folding path and an associated damping coefficient in order to achieve a target energy gap while minimizing the vibration in the post-folding phase at the same time. These results

confirm that choosing the folding path is essential for controlling the folding behaviors of deployable structures.

It is worth noting that here, we have only briefly touched upon the dynamic behaviors of the folding process of the meta-ribbon. More detailed analyses are needed to quantify the folding dynamics, as well as the relationship between the dissipation of vibration and the damping of the system. Furthermore, although the accuracy of the discrete numerical framework and the theoretical model for describing the static behaviors of elastic ribbons has been verified by experiments,[50,51] cross-validation from experiments for the dynamic folding is still missing and will be conducted using a high-speed camera and a 3D scanner in future studies.

Multistable states

In the previous investigation, we notice that the introduction of kinks and creases breaks the rotational symmetry of the (ring-shape) meta-ribbon, which leads to a finite number of stable states in the buckled meta-ribbon with a saddle shape. In this section, we discuss the existence and transformations of multistable configurations in kink-induced elastic polygonal ribbons and creased annular ribbons in detail.

We first consider an elastic polygonal ribbon with kinks $N^c = 8$ and $\psi = 80^\circ$, which buckles into a saddle-like configuration, as shown in Figure 6A. We apply vertical displacement (d) to the midpoints of two sides following the blue arrows. At the same time, the midpoints (red) of two different sides are constrained to slide along the dashed line that connects the two points. With the increase of d, the configuration of the buckled saddle-like polygonal ribbon transforms accordingly. We record the evolution of the total elastic energy of the system (E) as well as the reaction force (F) during the loading process and plot them as a function of the d in Figures 6B and 6C, respectively. The representative configurations are presented in Figure 6A. The first, third, and fifth configurations correspond to a stable equilibrium, identical in shape except for a rigid body rotation; however, the second and the fourth shapes have unstable equilibrium and will jump back to the stable equilibrium once the constraints are released. The overall configuration transformation can be found in Video S7.

Next, the multistability of an elastic annular ribbon is explored in a manner similar to the previous polygonal ribbon. Again, an annular ribbon with creases $N_c = 8$ and $\phi = 80^\circ$ is investigated, and the boundary and loading conditions are identical to the previous scenario. Figure 6D presents five equilibrium configurations during the transformation process, and analogously, three of them are stable and the other two are unstable. The associated E-d relationship and F-d curve are plotted in Figures 6E and 6F, respectively. The configuration transformation for this case is available in Video S8. From the above investigation, we can notice that there are abundant multistable behaviors in the foldable structures, although we only discussed the tri-stable states in the 8-side elastic polygon and creased annulus as basic examples. It can be expected that more complex multistable structures can be obtained by choosing the number of folds (kinks and/or creases),[33,34] and these structures may play significant roles in a wide range of applications, such as morphing structures[52,53] and robotic matters.[14,15]

DISCUSSION

Through discrete modeling, theoretical analysis, and tabletop experiments, we have uncovered the folding mechanism of meta-ribbons through both in-plane kinks and

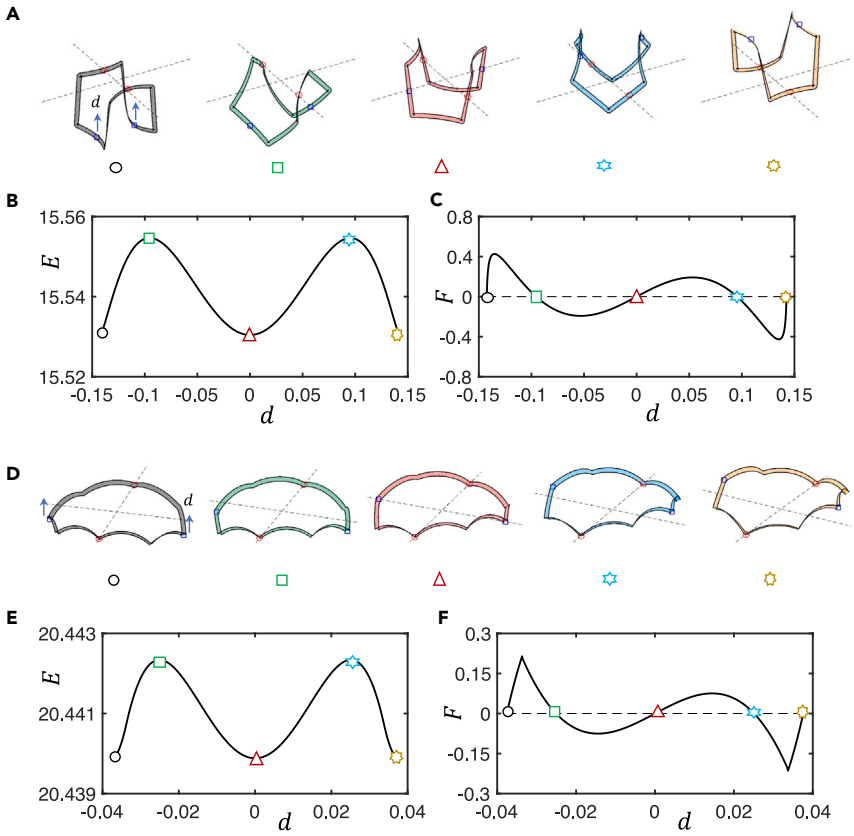

Figure 6. Transformations between multistable states in elastic meta-ribbons

(A–C) Elastic polygonal ribbon with kinks $N^c = 8$ and $\psi = 80°$: (A) representative equilibrium configurations during the actuating process, (B) the total energy, E, as a function of the actuation displacement, d, and (C) the force-displacement ($F - d$) curve.

(D–F) Annular ribbon with creases $N_c = 8$ and $\phi = 80°$: (D) representative equilibrium configurations during the actuating process, (E) the total energy, E, as a function of the actuation displacement, d, and (F) the force-displacement ($F - d$) curve.

out-of-plane creases. Folds are widely adopted in deployable/foldable structures, such as origami and kirigami. The deformation of single or multiple folds can be modeled as discrete hinges with appropriate boundary conditions or continuous structures by the regularized Heaviside or Dirac delta function.[48,54] In the current study, a discrete numerical model is employed to study the nonlinear mechanics of ribbons with kinks and creases, which are treated naturally in the discrete framework. We found that the folding of elastic polygonal ribbons with kinks is continuous and governed by a supercritical bifurcation, while the folding of annular ribbons with creases results in snapping folding and is controlled by a subcritical bifurcation. The folding behavior for the polygonal ribbon is governed by the total folding angle, ψN^c, which is similar to the looping behavior of a circular strip. In addition, the elastic energy E of a creased annular ribbon is found to be proportional to $(N_c - 2)^2$. Moreover, if both in-plane kinks and out-of-plane creases are integrated, then the folding process of a ring-shape meta-ribbon can be tunable, e.g., an appropriate energy landscape can be precisely selected to achieve a desired folding behavior. We further show the multistability and associated transformation in the meta-ribbon with a saddle-like shape, in which the rotational symmetry of a ring shape breaks, and the continuous family in a buckled saddle shape becomes a finite number of stable patterns. Our results illustrate the utility of our methods and findings,

establishing them as a promising asset in a broad range of applications, from fundamental physics analysis to novel meta-material designs, as well as the development of functional structures in practical engineering.

EXPERIMENTAL PROCEDURES

Resource availability

Lead contact

Further information and requests for resources and materials should be directed to and will be fulfilled by the lead contact, Mingchao Liu (m.liu.2@bham.ac.uk).

Materials availability

No materials were produced in this work.

Data and code availability

Data and code utilized in this study are available from the lead contact upon request.

Discrete model

We first introduced the discrete numerical framework for the nonlinear mechanical analysis of C^0 continuous strips with in-plane kinks and out-of-plane creases. Previous discrete differential geometry-based numerical frameworks for deployable structures usually focus on a continuous system, e.g., ribbons,[55] umbrella meshes,[56] and gridshells,[57] where smooth curvatures are used to describe the deformation. Here, we develop a general discrete model that can handle a mechanical system consisting of both continuous curvatures and local discontinuities. This discrete rod model is suited for the analysis of slender strips with sudden changes in rotation and curvature, which is the case for the meta-ribbon studied here. The centerline of a continuous closed-loop strip is first discretized into N nodes, $[\mathbf{x}_0,\mathbf{x}_1,\ldots,\mathbf{x}_{N-1}]$, and N edge vectors, $[\mathbf{e}^0,\mathbf{e}^1,\ldots,\mathbf{e}^{N-1}]$. To capture the orientation and the rotation of each edge element, $\mathbf{e}^i$, an orthonormal reference frame $\{\mathbf{d}_1^i,\mathbf{d}_2^i,\mathbf{d}_3^i\}$ and a material frame $\{\mathbf{m}_1^i,\mathbf{m}_2^i,\mathbf{m}_3^i\}$ are constructed (see Figures 7A and 7B for details). It should be noted that both frames share the tangent $\mathbf{d}_3^i \equiv \mathbf{m}_3^i = \mathbf{e}^i / \|\mathbf{e}^i\|$ as one of the directors, i.e., the frames remain adapted to the centerline. Similarly, the first material director, $\mathbf{m}_1^i$, is the surface normal of the elastic ribbon, and $\mathbf{m}_2^i = \mathbf{m}_3^i \times \mathbf{m}_1^i$ is along the ribbon width direction. The reference frame is updated through time parallel transport,[46,47] and the material frame can be later obtained from the reference frame using a scalar twist angle θ^i. This implies that the rod centerline can be represented using a $4N$-sized ($3N$ for the nodal coordinates and N for twist angles) degree of freedom vector

$$\mathbf{q} = \left[\mathbf{x}_0,\theta^0,\mathbf{x}_1,\theta^1,\ldots,\mathbf{x}_{N-1},\theta^{N-1}\right]. \qquad \text{(Equation 4)}$$

The strains of an elastic ribbon are comprised of three parts: stretching, bending, and twisting. Stretching strain associated with the i-th edge, $\mathbf{e}^i$, is

$$\epsilon^i = \frac{\|\mathbf{e}^i\|}{\|\bar{\mathbf{e}}^i\|} - 1, \qquad \text{(Equation 5)}$$

and, hereafter, a bar on the top indicates the quantity evaluated in the stress-free configurations, and $\|\circ\|$ refers to the $\mathcal{L}_2$ norm of a vector. Bending strain is captured by the curvature binormal, which measures the misalignment between two consecutive edges at a node $\mathbf{x}_i$,

$$(\kappa\mathbf{b})_i = \frac{2\mathbf{e}^{i-1}\times\mathbf{e}^i}{\|\mathbf{e}^{i-1}\|\|\mathbf{e}^i\| + \mathbf{e}^{i-1}\cdot\mathbf{e}^i}, \qquad \text{(Equation 6)}$$

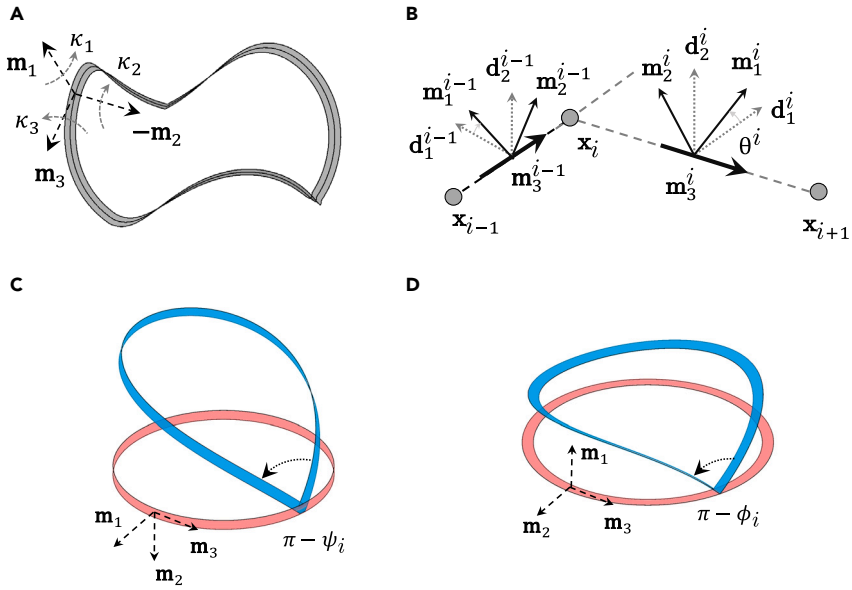

Figure 7. Model description

(A) Diagram of an annular ribbon.

(B) A discrete element for the 1D elastic body.

(C) Folding a circular strip through an in-plane kink.

(D) Folding an annular ribbon through an out-of-plane crease.

and the material curvatures are given by the inner products between the curvature binormal and material frame vectors,

$$\kappa_{1,i} = \frac{1}{2}\frac{\left(\mathbf{m}_2^{i-1}+\mathbf{m}_2^{i}\right)\cdot(\kappa\mathbf{b})_i}{\Delta l_i} \text{ and}$$
$$\kappa_{2,i} = -\frac{1}{2}\frac{\left(\mathbf{m}_1^{i-1}+\mathbf{m}_1^{i}\right)\cdot(\kappa\mathbf{b})_i}{\Delta l_i}, \quad \text{(Equation 7)}$$

with $\Delta l_i = (\| \mathbf{e}^i \| + \| \mathbf{e}^{i+1} \|)/2$, where $\kappa_{1,i}$ is the in-plane curvature, $\kappa_{2,i}$ is the out-of-plane curvature, and Δl_i is its Voronoi length. The twisting strain at the i-th node, in the discrete setting of DER, is measured using the discrete twist.[50,51]

$$\kappa_{3,i} = \frac{\theta^i - \theta^{i-1} + m_i^{\text{ref}}}{\Delta l_i}, \quad \text{(Equation 8)}$$

where m_i^{ref} is the reference twist associated with the reference frame and can be updated through a time parallel algorithm.[46,47]

The discrete energies are the quadratic form of the strains formulated before,

$$E^{\text{s}} = \sum_{i=0}^{N-1}\frac{1}{2}EA^i\left(\epsilon^i\right)^2 \| \bar{\mathbf{e}}^i \|,$$
$$E_1^{\text{b}} = \sum_{i=0}^{N-1}\frac{1}{2}EI_{1,i}(\kappa_{1,i} - \bar{\kappa}_{1,i})^2\Delta l_i,$$
$$E_2^{\text{b}} = \sum_{i=0}^{N-1}\frac{1}{2}EI_{2,i}(\kappa_{2,i} - \bar{\kappa}_{2,i})^2\Delta l_i, \text{and} \quad \text{(Equation 9)}$$
$$E^{\text{t}} = \sum_{i=0}^{N-1}\frac{1}{2}GJ_i(\kappa_{3,i} - \bar{\kappa}_{3,i})^2\Delta l_i,$$

where EA^i is the stretching stiffness, $EI_{1,i}$ (and $EI_{2,i}$) is the bending stiffness, and GJ_i is the twisting stiffness. For a slender ribbon, EA is usually much larger compared to all other stiffness parameters, such that the stretching energy performs like a penalty energy to ensure the inextensibility of the ribbon centerline. Therefore, the total energy can be calculated from Equation 1.

The discontinuity can be naturally included within the discrete model, as our computational framework is discrete with C^0 continuous. As shown in Figure 7C, if a kink with turning angle ψ_i is introduced into the i-th node, $\mathbf{x}_i$, then the equivalent in-plane curvature is defined by Equation 2, and its bending stiffness $EI_{1,i}$ is set to be a sufficiently large number and performs like a Lagrange multiplier to ensure that $\kappa_{1,i} = \bar{\kappa}_{1,i}$. On the other hand, as shown in Figure 7D, the crease is also achieved in a manner similar to the kink, i.e., the out-of-plane curvature is defined by Equation 3, and $EI_{2,i}$ is increased simultaneously to realize $\kappa_{2,i} = \bar{\kappa}_{2,i}$.

Finally, to get the stable equilibrium configuration of the deformed annulus, the dynamic relaxation method is employed to solve the nonlinear governing equations, i.e., the inertial and damping forces are considered, and the governing equations are dynamic, i.e., based on the statement of force balance, the implicit Euler method is used to solve the discrete dynamic equations of motion and update the degree of freedom (DOF) vector from $t = t_k$ to $t = t_{k+1}$,

$$\begin{aligned} &\mathbb{M}\ddot{\mathbf{q}}(t_{k+1}) - \mathbf{F}^{\text{ela}}(t_{k+1}) - \mathbf{F}^{\text{dam}}(t_{k+1}) = 0, \\ &\mathbf{q}(t_{k+1}) = \mathbf{q}(t_k) + \dot{\mathbf{q}}(t_{k+1})\,\Delta t, \text{and} \\ &\dot{\mathbf{q}}(t_{k+1}) = \dot{\mathbf{q}}(t_k) + \ddot{\mathbf{q}}(t_{k+1})\,\Delta t, \end{aligned} \qquad \text{(Equation 10)}$$

where $\mathbb{M}$ is the diagonal mass matrix, Δt is the time step size, $\mathbf{F}^{\text{ela}}$ is the elastic force vector and can be computed by taking the discrete variation of Equation 9, and $\mathbf{F}^{\text{dam}}$ is the damping force vector and can be formulated based on the Rayleigh matrix,

$$\mathbf{F}^{\text{dam}} = -(\alpha\mathbb{M} + \beta\mathbb{K})\dot{\mathbf{q}}, \qquad \text{(Equation 11)}$$

where α represents the damping drag during the rigid body motion and β is related to the viscoelasticity during the structural deformation. This numerical solver can robustly capture the discontinuities (e.g., fold point or snap point) and get the stable equilibrium automatically, without checking the eigenvalues/eigenvectors step by step, which would be extremely time consuming.[42] The gradient (associated with the internal elastic force) and the Hession (associated with the tangential stiffness matrix) are derived analytically based on discrete differential geometry, resulting in a fully implicit numerical framework for the nonlinear analysis of the meta-ribbon.

For the static analysis, we use the dynamic relaxation method to capture the static equilibrium, i.e., a suitable damping coefficient is selected to ensure the kinetic energy can be dissipated quickly; for the dynamic analysis, a physically valid damping coefficient is adopted for the real dynamic prediction. It should also be noted that collisions and frictional contact are inevitable during folding. However, these are ignored in our numerical model, given that the thickness of the ribbon strip is sufficiently small and our main focus is on the most fundamental nonlinear geometric and mechanical principles of folding. Additionally, we anticipate that the friction effect can be incorporated into our framework, as it has already been realized in the one-dimensional (1D) discrete simulation.[55,58]

Continuous model

We also employ a continuous model for theoretical analysis and cross-validation,[48] which is based on the anisotropic Kirchhoff rod theory.[59] Forces and moments are

decomposed into an orthogonal material frame attached to the centerline of the strip. Bending and twisting strains of the strip are then associated with the kinematic motion of the material frame along the centerline. We assume linear constitutive laws and obtain equilibrium equations regarding the forces and moments as a set of first-order ordinary differential equations (ODEs). We further employ the continuous description of creases in Yu et al.[48] to address the discontinuity of angles in creases, which use several Δ functions to describe the rest curvature of the creased annuli.[48] The continuation package AUTO 07P is used to solve the ODEs with associated boundary conditions.[60] Details are documented in supplemental experimental procedures section 2. Note that the anisotropic Kirchhoff rod model is accurate enough for prediction as long as the dimensions of the elastic structure satisfy the slender characteristics, i.e., $l \gg w \gg t$ and $l/w \gg w/t$.[50,51,61]

Experimental setup

The fabrication process is similar to the one presented in Yu et al.[48] Firstly, we laser cut elastic sheets into strips with different shapes, during which the desired in-plane kink angle can be directly introduced. To construct ribbons with out-of-plane angle, we mark the location of each crease and push it onto the edge of a rigid block with a particular angle to form the crease. We then employ an annealing technique to eliminate residual stress in the crease area and induce elastic creases. The annealing process involves heating the ribbon with creases above its glass transition temperature and then cooling it down to room temperature. Finally, we connect the cut and annealed strips with glue to form a closed loop. To achieve precise gluing of the two ends of annular strips, we utilize tools comprising a series of circular grooves. This allows the two ends of the elastic strip to securely fit inside the groove. Although the thickness of the joint area doubles, its impact on the nonlinear mechanical response of the creased strips is negligible due to its small length compared to the whole system. The sample size has a width w = 5.0 mm and a thickness t = 0.25 mm. The length is chosen to ensure the ring's size is suitable, preventing it from being too large to be affected by gravity or too small to cause visible plastic deformations in the materials.

SUPPLEMENTAL INFORMATION

Supplemental information can be found online at https://doi.org/10.1016/j.matt.2024.04.031.

ACKNOWLEDGMENTS

This work was funded by the start-up funding from Newcastle University, UK (W.H.); National Science Foundation grant 2122269 (T.Y.); the Nanyang Technological University, Singapore, grant M4082428 (K.J.H.); Ministry of Education, Singapore, grant MOE-MOET32022-0002 (K.J.H.); the Presidential Postdoctoral Fellowship from Nanyang Technological University, Singapore (M.L.); and start-up funding from the University of Birmingham, UK (M.L.). We are grateful to Dominic Vella, Zhaohe Dai, and Ruike Renee Zhao for the useful discussions.

AUTHOR CONTRIBUTIONS

Conceptualization, W.H., T.Y., and M.L.; methodology, W.H., T.Y., and M.L.; experiments, W.H.; investigation, W.H., T.Y., K.J.H., S.A., and M.L.; visualization, W.H.; supervision, T.Y. and M.L.; writing – original draft, W.H., T.Y., and M.L.; writing – review & editing, W.H., T.Y., K.J.H., S.A., and M.L.

DECLARATION OF INTERESTS

The authors declare no competing interests.

DECLARATION OF GENERATIVE AI AND AI-ASSISTED TECHNOLOGIES IN THE WRITING PROCESS

During the preparation of this work, the authors used ChatGPT to improve the language and readability of the manuscript. After using this service, the authors reviewed and edited the content as needed and took full responsibility for the content of the publication.

Received: November 15, 2023
Revised: January 29, 2024
Accepted: April 17, 2024
Published: May 15, 2024

REFERENCES

1. Pocivavsek, L., Dellsy, R., Kern, A., Johnson, S., Lin, B., Lee, K.Y.C., and Cerda, E. (2008). Stress and fold localization in thin elastic membranes. Science *320*, 912–916.
2. Liu, Z., Cui, A., Li, J., and Gu, C. (2019). Folding 2D structures into 3D configurations at the micro/nanoscale: Principles, techniques, and applications. Adv. Mater. *31*, 1802211.
3. Zan, G., Wu, T., Zhu, F., He, P., Cheng, Y., Chai, S., Wang, Y., Huang, X., Zhang, W., Wan, Y., et al. (2021). A biomimetic conductive superfoldable material. Matter *4*, 3232–3247.
4. Dobson, C.M. (2003). Protein folding and misfolding. Nature *426*, 884–890.
5. Rothemund, P.W.K. (2006). Folding DNA to create nanoscale shapes and patterns. Nature *440*, 297–302.
6. Schenk, M., and Guest, S.D. (2011). Origami folding: A structural engineering approach. Origami *5*, 291–304.
7. Peraza-Hernandez, E.A., Hartl, D.J., Malak Jr, R.J., and Lagoudas, D.C. (2014). Origami-inspired active structures: A synthesis and review. Smart Mater. Struct. *23*, 094001.
8. Liu, K., Tachi, T., and Paulino, G.H. (2019). Invariant and smooth limit of discrete geometry folded from bistable origami leading to multistable metasurfaces. Nat. Commun. *10*, 4238.
9. Croll, A.B., Twohig, T., and Elder, T. (2019). The compressive strength of crumpled matter. Nat. Commun. *10*, 1502.
10. Li, S., Fang, H., Sadeghi, S., Bhovad, P., and Wang, K.-W. (2019). Architected origami materials: How folding creates sophisticated mechanical properties. Adv. Mater. *31*, 1805282.
11. Kuribayashi, K., Tsuchiya, K., You, Z., Tomus, D., Umemoto, M., Ito, T., and Sasaki, M. (2006). Self-deployable origami stent grafts as a biomedical application of ni-rich tini shape memory alloy foil. Mater. Sci. Eng., A *419*, 131–137.
12. Schenk, M., Viquerat, A.D., Seffen, K.A., and Guest, S.D. (2014). Review of inflatable booms for deployable space structures: Packing and rigidization. J. Spacecraft Rockets *51*, 762–778.
13. Coulais, C., Sabbadini, A., Vink, F., and van Hecke, M. (2018). Multi-step self-guided pathways for shape-changing metamaterials. Nature *561*, 512–515.
14. Meng, Z., Liu, M., Yan, H., Genin, G.M., and Chen, C.Q. (2022). Deployable mechanical metamaterials with multistep programmable transformation. Sci. Adv. *8*, eabn5460.
15. Yang, X., Zhou, Y., Zhao, H., Huang, W., Wang, Y., Hsia, K.J., and Liu, M. (2023). Morphing matter: From mechanical principles to robotic applications. Soft Sci. *3*, 38.
16. Chan, H.S., and Dill, K.A. (1993). The protein folding problem. Phys. Today *46*, 24–32.
17. Schneider, F., Möritz, N., and Dietz, H. (2019). The sequence of events during folding of a DNA origami. Sci. Adv. *5*, eaaw1412.
18. Garcia, K.E., Wang, X., and Kroenke, C.D. (2021). A model of tension-induced fiber growth predicts white matter organization during brain folding. Nat. Commun. *12*, 6681.
19. Shekhar, M., Terashi, G., Gupta, C., Sarkar, D., Debussche, G., Sisco, N.J., Nguyen, J., Mondal, A., Vant, J., Fromme, P., et al. (2021). Cryofold: Determining protein structures and data-guided ensembles from cryo-em density maps. Matter *4*, 3195–3216.
20. McRae, E.K.S., Rasmussen, H.Ø., Liu, J., Bøggild, A., Nguyen, M.T.A., Sampedro Vallina, N., Boesen, T., Pedersen, J.S., Ren, G., Geary, C., and Andersen, E.S. (2023). Structure, folding and flexibility of co-transcriptional RNA origami. Nat. Nanotechnol. *18*, 808–817.
21. Eisner, T. (1981). Leaf folding in a sensitive plant: A defensive thorn-exposure mechanism? Proc. Natl. Acad. Sci. USA *78*, 402–404.
22. De Focatiis, D.S.A., and Guest, S.D. (2002). Deployable membranes designed from folding tree leaves. Philos. Trans. A Math. Phys. Eng. Sci. *360*, 227–238.
23. Saito, K., Yamamoto, S., Maruyama, M., and Okabe, Y. (2014). Asymmetric hindwing foldings in rove beetles. Proc. Natl. Acad. Sci. USA *111*, 16349–16352.
24. Guo, K., Huang, C., Miao, Y., Cosgrove, D.J., and Hsia, K.J. (2022). Leaf morphogenesis: The multifaceted roles of mechanics. Mol. Plant *15*, 1098–1119.
25. Silverberg, J.L., Evans, A.A., McLeod, L., Hayward, R.C., Hull, T., Santangelo, C.D., and Cohen, I. (2014). Using origami design principles to fold reprogrammable mechanical metamaterials. Science *345*, 647–650.
26. Santangelo, C.D. (2017). Extreme mechanics: Self-folding origami. Annu. Rev. Condens. Matter Phys. *8*, 165–183.
27. Abdullah, A.M., Li, X., Braun, P.V., Rogers, J.A., and Hsia, K.J. (2018). Self-folded gripper-like architectures from stimuli-responsive bilayers. Adv. Mater. *30*, 1801669.
28. Abdullah, A.M., Li, X., Braun, P.V., Rogers, J.A., and Hsia, K.J. (2020). Kirigami-inspired self-assembly of 3d structures. Adv. Funct. Mater. *30*, 1909888.
29. Mouthuy, P.-O., Coulombier, M., Pardoen, T., Raskin, J.-P., and Jonas, A.M. (2012). Overcurvature describes the buckling and folding of rings from curved origami to foldable tents. Nat. Commun. *3*, 1290.
30. Wu, S., Yue, L., Jin, Y., Sun, X., Zemelka, C., Qi, H.J., and Zhao, R. (2021). Ring origami: Snap-folding of rings with different geometries. Advanced Intelligent Systems *3*, 2100107.
31. Wu, S., Dai, J., Leanza, S., and Zhao, R.R. (2022). Hexagonal ring origami—snap-folding with large packing ratio. Extreme Mechanics Letters *53*, 101713.
32. Lu, L., Leanza, S., Dai, J., Sun, X., and Zhao, R.R. (2023). Easy snap-folding of hexagonal ring origami by geometric modifications. J. Mech. Phys. Solid. *171*, 105142.
33. Lu, L., Dai, J., Leanza, S., Zhao, R.R., and Hutchinson, J.W. (2023). Multiple equilibrium states of a curved-sided hexagram: Part I — Stability of states. J. Mech. Phys. Solid. *180*, 105406.

34. Lu, L., Dai, J., Leanza, S., Hutchinson, J.W., and Zhao, R.R. (2023). Multiple equilibrium states of a curved-sided hexagram: Part II — Transitions between states. J. Mech. Phys. Solid. *180*, 105407.

35. Dias, M.A., Dudte, L.H., Mahadevan, L., and Santangelo, C.D. (2012). Geometric mechanics of curved crease origami. Phys. Rev. Lett. *109*, 114301.

36. Dias, M.A., and Audoly, B. (2014). A non-linear rod model for folded elastic strips. J. Mech. Phys. Solid. *62*, 57–80.

37. Liu, Y., Shaw, B., Dickey, M.D., and Genzer, J. (2017). Sequential self-folding of polymer sheets. Sci. Adv. *3*, e1602417.

38. Bende, N.P., Evans, A.A., Innes-Gold, S., Marin, L.A., Cohen, I., Hayward, R.C., and Santangelo, C.D. (2015). Geometrically controlled snapping transitions in shells with curved creases. Proc. Natl. Acad. Sci. USA *112*, 11175–11180.

39. Araújo, N.A.M., da Costa, R.A., Dorogovtsev, S.N., and Mendes, J.F.F. (2018). Finding the optimal nets for self-folding kirigami. Phys. Rev. Lett. *120*, 188001.

40. Bambic, M.P., Araújo, N.A., Walker, B.J., Hewitt, D.R., Pei, Q.X., Ni, R., and Volpe, G. (2023). Optimal face-to-face coupling for fast self-folding kirigami. Preprint at arXiv. https://doi.org/10.48550/arXiv.2005.08202.

41. Liu, M., Gomez, M., and Vella, D. (2021). Delayed bifurcation in elastic snap-through instabilities. J. Mech. Phys. Solid. *151*, 104386.

42. Huang, W., Zhang, Y., Yu, T., and Liu, M. (2023). Bifurcations and stability analysis of elastic slender structures using static discrete elastic rods method. J. Appl. Mech. *90*.

43. Dai, L., Guan, F., and Guest, J.K. (2014). Structural optimization and model fabrication of a double-ring deployable antenna truss. Acta Astronaut. *94*, 843–851.

44. Liu, T.-W., Bai, J.-B., Fantuzzi, N., Xi, H.-T., Xu, H., Li, S.-L., and Cao, P.-C. (2023). Folding behavior of thin-walled tubular deployable composite boom for space applications: Experiments and numerical simulation. Acta Astronaut. *209*, 159–171.

45. Chen, Y., Feng, H., Ma, J., Peng, R., and You, Z. (2016). Symmetric waterbomb origami. Proc. Math. Phys. Eng. Sci. *472*, 20150846.

46. Bergou, M., Wardetzky, M., Robinson, S., Audoly, B., and Grinspun, E. (2008). Discrete elastic rods. In ACM Transactions on Graphics (TOG), *27*ACM Transactions on Graphics (TOG) (ACM), p. 63.

47. Bergou, M., Audoly, B., Vouga, E., Wardetzky, M., and Grinspun, E. (2010). Discrete viscous threads. In ACM Transactions on Graphics (TOG), *29*ACM Transactions on Graphics (TOG), p. 1.

48. Yu, T., Marmo, F., Cesarano, P., and Adriaenssens, S. (2023). Continuous modeling of creased annuli with tunable bistable and looping behaviors. Proc. Natl. Acad. Sci. USA *120*, e2209048120.

49. Leanza, S., Zhao, R.R., and Hutchinson, J.W. (2023). On the elastic stability of folded rings in circular and straight states. Eur. J. Mech. Solid. 105041.

50. Audoly, B., and Neukirch, S. (2021). A one-dimensional model for elastic ribbons: a little stretching makes a big difference. J. Mech. Phys. Solid. *153*, 104457.

51. Huang, W., Ma, C., Chen, Q., and Qin, L. (2022). A discrete differential geometry-based numerical framework for extensible ribbons. Int. J. Solid Struct. *248*, 111619.

52. Yu, T., Dreier, L., Marmo, F., Gabriele, S., Parascho, S., and Adriaenssens, S. (2021). Numerical modeling of static equilibria and bifurcations in bigons and bigon rings. J. Mech. Phys. Solid. *152*, 104459.

53. Liu, M., Domino, L., Dupont de Dinechin, I., Taffetani, M., and Vella, D. (2023). Snap-induced morphing: From a single bistable shell to the origin of shape bifurcation in interacting shells. J. Mech. Phys. Solid. *170*, 105116.

54. Jules, T., Lechenault, F., and Adda-Bedia, M. (2019). Local mechanical description of an elastic fold. Soft Matter *15*, 1619–1626.

55. Baek, C., Martin, A.G., Poincloux, S., Chen, T., and Reis, P.M. (2021). Smooth triaxial weaving with naturally curved ribbons. Phys. Rev. Lett. *127*, 104301.

56. Ren, Y., Kusupati, U., Panetta, J., Isvoranu, F., Pellis, D., Chen, T., and Pauly, M. (2022). Umbrella meshes: elastic mechanisms for freeform shape deployment. ACM Trans. Graph. *41*, 1–15.

57. Panetta, J., Konaković-Luković, M., Isvoranu, F., Bouleau, E., and Pauly, M. (2019). X-shells: A new class of deployable beam structures. ACM Trans. Graph. *38*, 1–15.

58. Tong, D., Choi, A., Joo, J., and Jawed, M.K. (2023). A fully implicit method for robust frictional contact handling in elastic rods. Extreme Mechanics Letters *58*, 101924.

59. Audoly, B., and Pomeau, Y. (2010). Elasticity and Geometry: From Hair Curls to the Non-linear Response of Shells (Oxford University Press).

60. Doedel, E.J. (2007). Lecture notes on numerical analysis of nonlinear equations. In Numerical Continuation Methods for dynamical systems (Springer), pp. 1–49.

61. Huang, W., Wang, Y., Li, X., and Jawed, M.K. (2020). Shear induced supercritical pitchfork bifurcation of pre-buckled bands, from narrow strips to wide plates. J. Mech. Phys. Solid. *145*, 104168.